

Divalent 2-(4-Hydroxyphenyl)benzothiazole Bifunctional Chelators for ^{64}Cu Positron Emission Tomography Imaging in Alzheimer's Disease

Karna Terpstra,[○] Yujue Wang,[○] Truc T. Huynh, Nilantha Bandara, Hong-Jun Cho, Buck E. Rogers,* and Liviu M. Mirica*



Cite This: *Inorg. Chem.* 2022, 61, 20326–20336



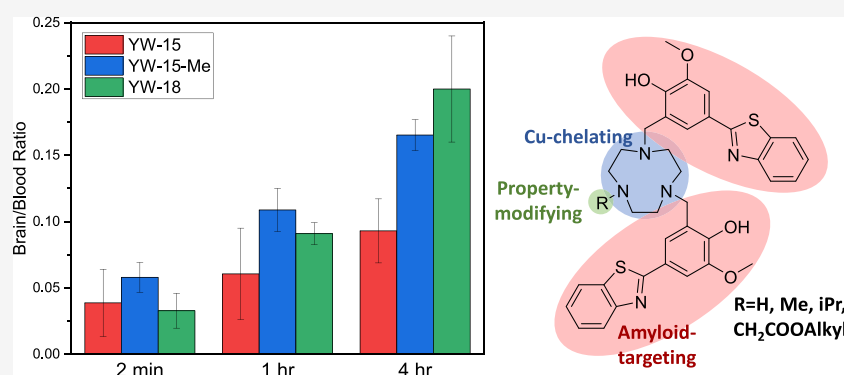
Read Online

ACCESS |

Metrics & More

Article Recommendations

Supporting Information



ABSTRACT: Herein, we report a new series of divalent 2-(4-hydroxyphenyl)benzothiazole bifunctional chelators (BFCs) with high affinity for amyloid β aggregates and favorable lipophilicity for blood–brain barrier penetration. The addition of an alkyl carboxylate pendant arm offers high binding affinity toward Cu(II) . The novel BFCs form stable ^{64}Cu -radiolabeled complexes and exhibit promising partition coefficient ($\log D$) values of 1.05–1.85. Among the five compounds tested, the ^{64}Cu -YW-15 complex exhibits significant staining of amyloid β plaques in *ex vivo* autoradiography studies. In addition, biodistribution studies show that ^{64}Cu -YW-15-Me exhibits moderate brain uptake (0.69 ± 0.08 %ID/g) in wild type mice.

INTRODUCTION

Alzheimer's disease (AD) is the most common cause of dementia. The formation of extracellular amyloid plaques in the brain, caused by accumulation of misfolded amyloid β ($A\beta$) peptides, is a primary hallmark of AD progression.^{1–4} As a characteristic biomarker of AD, amyloid plaques have been used as a standard diagnostic target for decades. Effective measurement of amyloid plaque burden in patient brains could be an asset for early diagnosis of AD.^{5–7}

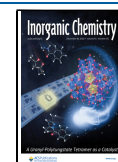
Positron emission tomography (PET) is a molecular imaging technique that allows for noninvasive evaluation of amyloid plaque burden in the brain by utilizing imaging agents that contain positron-emitting radioisotopes.^{6,8} Amyloid imaging probes that utilize short lived radionuclides such as ^{11}C ($t_{1/2} = 20$ min) and ^{18}F ($t_{1/2} = 110$ min) including ^{18}F -florbetaben have been investigated extensively and applied in the clinic.^{9–14} However, these radioisotopes are attached to target agents via covalent bonding, which normally requires special reaction conditions and equipment.¹⁵ Incorporating a radiometal rapidly into an imaging agent can be a convenient alternative. Several high-affinity ligands such as diacetyl-bis(N^4 -methylthiosemicarbazone (ATSM), 1,4,7,10-tetraazacyclodo-

decane (cyclen), and 1,4,7-triazacyclononane (TACN) derivatives have been developed as molecular imaging agents that utilize radiotracers such as ^{64}Cu ($t_{1/2} = 12.7$ h).^{16–20}

Our research group has previously reported TACN-based $A\beta$ -targeting bifunctional chelators (BFCs) for potential ^{64}Cu PET imaging applications^{21–27} and recently for ^{68}Ga PET imaging of $A\beta$ deposits on blood vessels in cerebral amyloid angiopathy (CAA).²⁸ We have reported ^{64}Cu complexes with moderate to good blood–brain barrier (BBB) permeability over 1 %ID/g,^{22,23} in comparison to 4.77 %ID/g that was measured for FDA-approved radiotracer ^{18}F -florbetaben.¹⁴ These BFCs and their Cu complexes have shown mid-nanomolar affinity for amyloid plaques,^{22,24,25} in comparison to the 6.7 nM K_i of ^{18}F -florbetaben.¹⁴ We have also previously

Received: July 31, 2022

Published: December 4, 2022



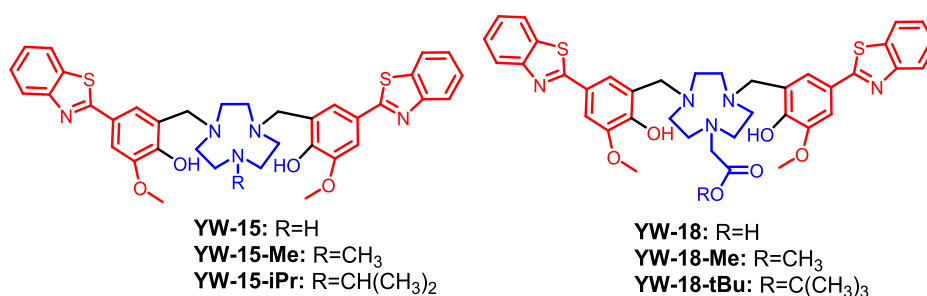


Figure 1. Structures of BFCs investigated herein. The metal-binding and A β -interacting fragments are shown in blue and red, respectively.

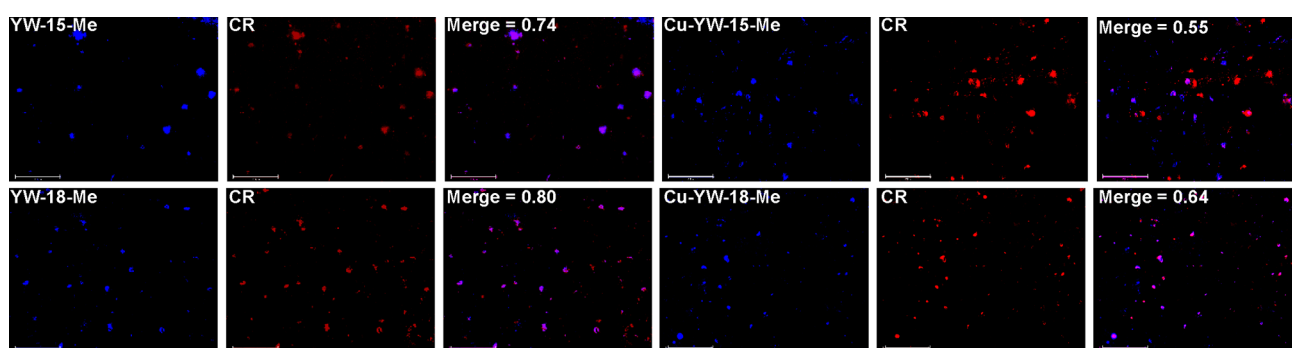


Figure 2. Fluorescence microscopy images of 5xFAD mouse brain sections incubated with compounds YW-15-Me, YW-18-Me, and their Cu(II) complexes (50 μ M), Congo Red (2 μ M, CR), and merged images (R = Pearson's coefficient). Magnification: 20 \times . Scale bar: 125 μ m.

reported BFCs with high stability constants for their Cu complexes, approaching values similar to 1,4,7-triazacyclononane-1,4,7-triacetic acid (NOTA),^{21,26,27,29} thus indicating that the class of TACN-based BFCs is promising in the development of ⁶⁴Cu PET imaging agents for AD.

Despite the promise of these complexes, further optimization of at least one of the three properties described above is required for each ligand system prior to further investigation. We consider that careful optimization of the previously developed BFCs can have major impacts on their properties. A broad comparison of how specific structural changes aimed at optimizing a single property impacts the other properties would serve as a guide for ligand optimization in the future.

Herein, we report a series of BFCs containing two A β -targeting fragments and a TACN macrocyclic ligand, along with novel derivatives containing carboxylate ester arms to increase their lipophilicity and improve BBB permeability.³⁰ In addition, the BFCs YW-15 and YW-18 are analyzed for the first time as ligands of copper for the labeling of amyloid plaques, which is different than their utilization as ⁶⁸Ga ligands to image CAA.²⁸ Along with the previously reported TACN-based ligands,^{26–28} the analysis of the current BFCs provides a deeper understanding of the impact of ligand structural modifications onto the changes in amyloid affinity, lipophilicity, metal complex stability, biodistribution profile, and ultimately *in vivo* applications.

RESULTS AND DISCUSSION

Design and Synthesis of BFCs. The BFCs discussed herein were generated using a synthetic route based on a Mannich reaction between 2-(4-hydroxy-3-methoxyphenyl)-benzothiazole and TACN in the presence of paraformaldehyde (Figure 1). A second identical A β -binding fragment was added to the BFC framework to improve the affinity for the amyloid plaques. In BFCs YW-15-Me and YW-15-iPr, alkyl sub-

stituents were added to the TACN backbone, in contrast to the parent secondary amine derivative YW-15,²⁸ while in BFCs YW-18-Me and YW-18-tBu, a pendant carboxylate arm was added via reactions with methyl and *tert*-butyl bromoacetate, respectively, to increase the metal chelation ability of the corresponding BFC. Hydrolysis of YW-18-tBu in the presence of concentrated hydrochloric acid generates YW-18, a carboxylic acid-containing BFC that should act as the strongest metal chelator among this series. Relevant to this work, BFCs YW-15 and YW-18 have recently been employed by our groups in the development of ⁶⁸Ga complexes for potential PET imaging of amyloid plaques deposited to blood vessels in cerebral amyloid angiopathy (CAA).²⁸

Fluorescence Imaging of Amyloid Plaques in 5xFAD Mouse Brain Sections. *Ex vivo* staining and imaging of 5xFAD mouse brain sections was conducted to evaluate the affinity of the BFCs toward A β species. Brain sections were collected from 9 to 11 month old 5xFAD mice, which have developed amyloid pathology found in AD.^{31,32} An appreciable amount of fluorescence staining was observed upon incubation of the brain sections for 30 min with 50 μ M solutions of BFCs and Cu(II) complexes, as demonstrated by the fluorescence images of YW-15-Me and YW-18-Me (Figure 2). The specific staining of amyloid plaques was confirmed by staining with 2 μ M Congo Red (CR), a commonly used amyloid-binding fluorescent dye (Figure 2).^{33,34} Fluorescence images of YW-15,²⁸ YW-15-iPr, and YW-18 also show that these BFCs specifically bind to amyloid plaques by co-staining with Congo Red and a significant degree of fluorescence colocalization (Figure S3).

To confirm the specific staining of A β plaques by BFCs and their Cu(II) complexes, the fluorescent dye AF 594-labeled antibody HJ3.4 was utilized for staining. This AF594-conjugated HJ3.4 antibody (AF594-HJ3.4) could bind to a wide range of A β species.^{23,35–39} Solutions of 50 μ M of BFCs

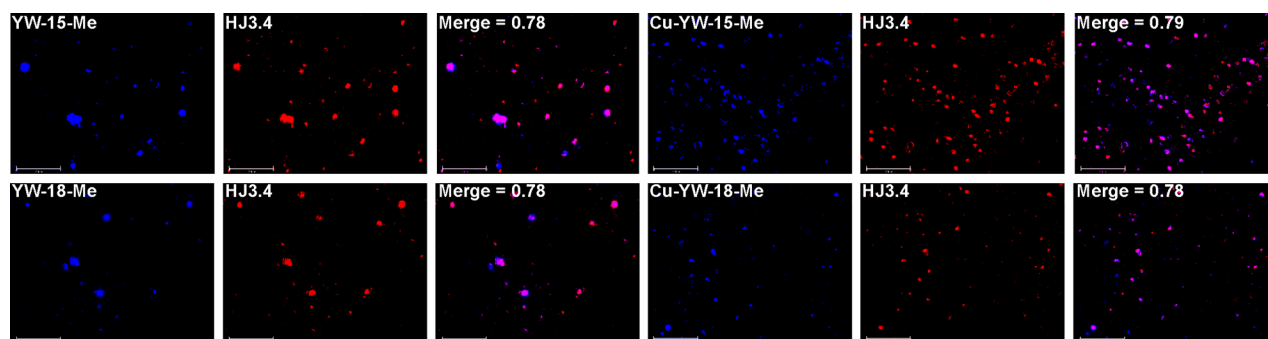


Figure 3. Fluorescence microscopy images of 5x FAD mouse brain sections incubated with YW-15-Me and YW-18-Me as well as their Cu(II) complexes (left panels), AF594-HJ3.4 (center panels), and merged images (right panels). Magnification: 20 \times . Scale bar: 125 μ m.

and their Cu(II) complexes were used to treat 6 to 11 month old 5x FAD mouse brain sections. A heavy load of A β -plaque emission signal by AF594-HJ3.4 showed favorable colocalization with the BFCs and their Cu(II) complexes, as suggested by the calculated Pearson's coefficients. An especially favorable colocalization was observed for BFCs YW-15-Me and YW-18-Me and their Cu(II) complexes (Figure 3), while a slightly reduced colocalization was observed for BFCs YW-15-iPr and YW-18-tBu (Figure S4). The extent of colocalization for AF594-HJ3.4 antibody is greater than that for CR, indicating that these BFCs bind to a wide range of soluble and insoluble A β species.

Quantification of BFC Affinity for Amyloid Plaques.

Thioflavin T (ThT) competition assays were utilized to determine the binding affinity of the BFCs containing two amyloid-targeting fragments toward synthetic amyloid plaques (Figure S5). An increase in fluorescence at 485 nm following excitation at 435 nm corresponds to increased concentration of ThT-associated amyloid plaques; decreased fluorescence indicates an increase in ligand association with amyloid plaques, from which the ThT has been displaced. YW-15, YW-18, and YW-18-Me were observed to have K_i values in the mid nM range at 290, 550, and 860 nM, respectively. YW-15-Me and YW-15-iPr were observed to have K_i values in the low μ M range, both at 1.3 μ M (Table 1). Overall, the ligands have moderate to high affinity for amyloid plaques, indicating potential for use as amyloid PET tracers.

Table 1. K_i Values Obtained for the BFCs from ThT Competition Assays for Binding to Amyloid Plaques

ligand	K_i (nM)
YW-15	290 \pm 60
YW-15-Me	1300 \pm 200
YW-15-iPr	1300 \pm 600
YW-18	550 \pm 90
YW-18-Me	860 \pm 250

Determination of Lipophilicity by LogD. LogD values were measured to predict the blood–brain barrier (BBB) permeability of BFCs. The determination of logD values of BFCs was conducted by fluorescence intensity measurement using conditions described in the experimental section (see Supporting Information). All BFCs other than YW-18 have logD values around or over 1.2 (Table 2), suggesting that these compounds have the potential to penetrate the BBB.^{40,41} A lower logD was obtained for the carboxylic acid YW-18, due to its increased hydrophilicity. Finally, since YW-18-tBu does not

Table 2. Molecular Weights (MWs) and Measured LogD Values for Each BFC

ligand	MWs (g·mol ⁻¹)	logD
YW-15	667.2	1.23 \pm 0.04
YW-15-Me	681.2	1.19 \pm 0.05
YW-15-iPr	709.9	1.30 \pm 0.03
YW-18	725.3	0.89 \pm 0.07
YW-18-Me	739.3	1.20 \pm 0.10
YW-18-tBu	782.3	1.22 \pm 0.04

exhibit a higher logD value than YW-18-Me and its molecular weight is higher, the YW-18-tBu BFC was not used in any subsequent *in vitro* and *in vivo* studies.

Stability Constants with Metal Ions by pH-Spectrophotometric Titration. The presence of several acidic and basic functional groups in each BFC prompted the determination of their acidity constants (pK_a) by UV–vis spectrophotometric titrations. Titration of YW-15 from pH 3 to 11 revealed several changes in the spectrum, including the disappearance of a 325 nm band and the appearance of a 375 nm shoulder with an isosbestic point at 350 nm (Figure 4). As the pH of the solution decreases, the 325 nm band continues to disappear with a shifted isosbestic point at 333 nm until the λ_{max} of the spectrum shifts to a 362 nm band at high pH. Titration of YW-18 from pH 3 to 11 revealed similar changes in the spectrum with several notable differences (Figure 4). The titration initially revealed a very similar disappearance of a 325 nm band, with a 360 nm shoulder appearing and isosbestic point at 350 nm. As the solution becomes more basic, the shoulder at 375 nm disappears, while the 325 nm band remains steady until the shoulder has disappeared. The 325 nm band gradually shifts to a new λ_{max} of 360 nm, where the band stabilizes at high pH. Titrations of YW-15-Me, YW-15-iPr, and YW-18-Me were conducted from pH 3 to 11 and revealed similar changes in the spectrum (Figure S7). The best fit of the data revealed 4 pK_a values for each ligand (Table 3), calculated by HypSpec (Protonic Software, UK) and confirmed by monitoring changes in wavelengths of known species as a function of pH. Based on previously reported acidity constants for phenols and amines, pK_{a1-3} were assigned to deprotonation of the TACN amine groups, and pK_{a4} was assigned to deprotonation of the phenol.^{21,29} Acidity constants for the thiazole and carboxylic acid were not determined; these groups are expected to be acidic, and therefore the acidity constants are likely located outside the pH range of the performed titrations. Species distribution plots (Figure 4) were created

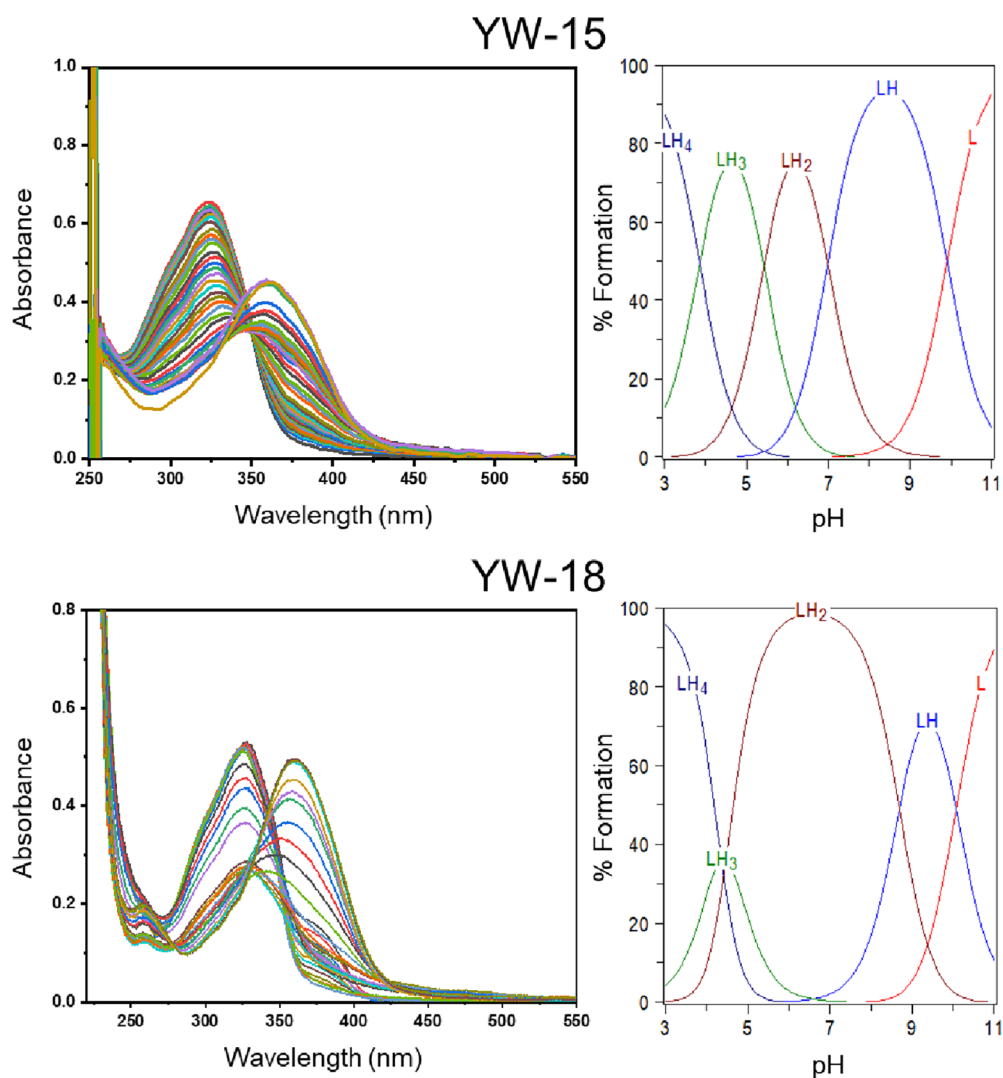


Figure 4. Variable pH UV-vis spectra of YW-15 and YW-18 (pH 3–11, [L] = 20 μ M, 25 $^{\circ}$ C, *I* = 0.1 M NaCl) and species distribution plots.

Table 3. Acidity Constants (pK_a) of BFCs Determined by Spectrophotometric Titrations (Errors for Last Digit)

reaction	YW-15	YW-15-Me	YW-15-iPr	YW-18	YW-18-Me
$[H_4L]^{3+} = [H_3L]^{2+} + H^+$ (pK_{a1})	3.86 (6)	3.53 (2)	4.18 (7)	4.37 (11)	2.06 (24)
$[H_3L]^{2+} = [H_2L]^+ + H^+$ (pK_{a2})	5.41 (4)	7.13 (1)	7.06 (6)	4.47 (11)	5.09 (4)
$[H_2L]^+ = [HL] + H^+$ (pK_{a3})	6.98 (2)	8.19 (1)	8.50 (4)	8.48 (11)	7.30 (2)
$[HL] = [L]^- + H^+$ (pK_{a4})	9.90 (1)	10.18 (1)	10.69 (3)	10.07 (7)	9.83 (1)

based the calculated pK_a values to show the % formation of each species of the ligand.

Quantification of the metal chelation ability of the BFCs was performed by spectrophotometric titration of the ligands in the presence of equimolar amounts of Cu(II). Titration of YW-15 pre-mixed with Cu(II) from pH 3 to 11 exhibits a gradual decrease in the 325 nm peak, which gradually stabilizes at an absorbance of approximately 0.25, before gradually shifting to a new λ_{max} of 345 nm, where the peak stabilizes at high pH (Figure 5). Titration of YW-18 in the presence of an equimolar amount of Cu(II) from pH 3 to 11 exhibits a gradual decrease in a 325 nm peak and appearance of a 420 nm shoulder with an isosbestic point at 350 nm. As the solution becomes more basic, the λ_{max} of the 325 nm peak gradually shifts to 375 nm, where the absorbance continues to decrease before stabilizing at high pH (Figure 5). Titrations of Cu-YW-15-Me, Cu-YW-

15-iPr, and Cu-YW-18-Me reveal similar trends as observed in Cu-YW-15 (Figure S8). The best fit of the data revealed $2\log K$ values for each ligand (Table 4), calculated by HypSpec (Protonic Software, UK) and confirmed by monitoring changes in wavelengths of known species as a function of pH.

The calculated stability constants reveal that the Cu(II) complex of monoprotonated YW-18 is approximately six orders of magnitude more stable than that of YW-15 (Table 4). We expect this is due to the presence of an additional metal-chelation carboxylate arm. Excitingly, the calculated stability constants of the complexes reveal similar stability to complexes known to have high copper affinity such as H₃nota and the previously published ⁶⁴Cu-based multifunctional complex CuL₁¹ which contains an ATSM ligand fragment (Table 4).^{29,42} By comparison, YW-15-iPr exhibits a more complicated speciation than the other BFCs, as the Jobs plot

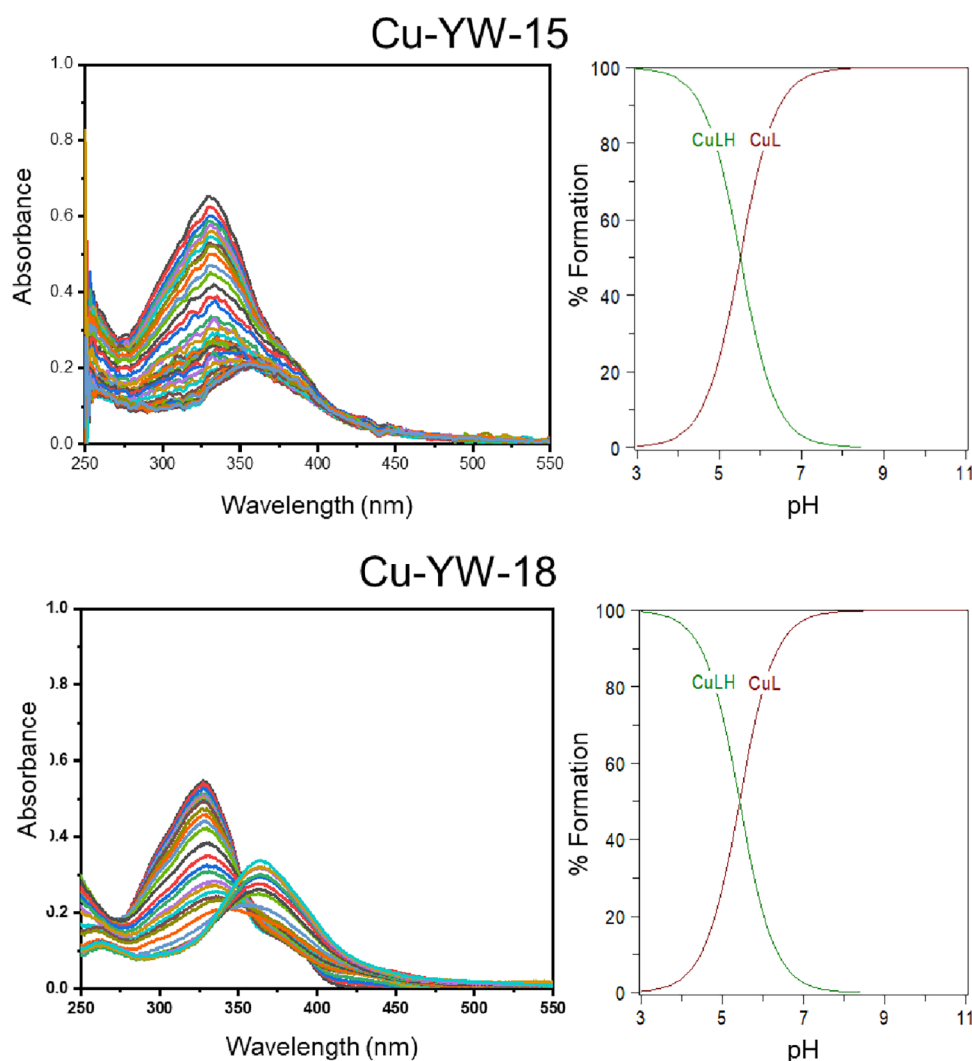


Figure 5. Variable pH UV-vis spectra of YW-15 and YW-18 copper complexes (pH 3–11, $[L] = [Cu^{2+}] = 20 \mu M$, $25^\circ C$, $I = 0.1 M NaCl$) and species distribution plots.

Table 4. Stability Constants (LogK) of the Cu(II) Complexes of YW-15 and YW-18

reaction	Cu-YW-15	Cu-YW-15-Me	Cu-YW-15-iPr	Cu-YW-18	Cu-YW-18-Me	CuL^{142}	H_3nota^{29}
$Cu^{2+} + LH = [CuLH]^{2+}$	5.51 (1)	7.18 (1)	7.19 (1)	5.42 (3)	8.10 (1)		2.74
$Cu^{2+} + L^- = [CuL]^+$	13.66 (1)	14.71 (1)	14.44 (1)	19.58 (2)	12.86 (1)	17.2	21.63

reveals the likely formation of a 2:1 ligand: Cu^{2+} complex (Figure S6). An additional titration of YW-15-iPr was conducted with a ratio of 2:1 ligand: Cu^{2+} (Figure S9), and the stability constants obtained from this titration indicate the presence of a CuL_2 complex (Table S1), thus confirming that the aqueous coordination chemistry of YW-15-iPr is more complicated than for the other BFCs.⁴³

Due to the presence of multiple Cu:L complexes present at physiological pH (Figure 5), an alternative method was employed to compare the chelating ability of the BFCs described herein. The pCu ($pCu = -\log[Cu_{free}]$) of each complex at a given pH allows for comparison of the amount of noncoordinated copper (Cu_{free}) present in solution, where higher pCu values indicate lower concentrations of Cu_{free} and therefore more copper coordinated by the BFCs and a higher Cu-BFC complex stability. Overall, the YW-18-based ligands have higher pCu values, closer to reported values of H_3nota , and therefore higher Cu-BFC complex stability at neutral pHs

than the YW-15-based ligands was expected based on the YW-18-based ligands containing an additional metal-chelating arm (Table 5).

Antioxidant Capacity of BFCs. The Cu^{2+} -induced antioxidant capacity (CIAC) assays were conducted to probe whether the BFCs described herein can control the undesired property of Cu^{2+} ions to promote a radical reaction under reducing conditions.^{25,43} CIAC assays measure radical

Table 5. pCu ($pCu = -\log[Cu_{free}]$) Values of Titration Solutions of Cu-YW-15, Cu-YW-15-Me, Cu-YW-15-iPr, Cu-YW-18, and Cu-YW-18-Me ($[L] = [Cu] = 20 \mu M$)

pH	Cu-YW-15	Cu-YW-15-Me	Cu-YW-15-iPr	Cu-YW-18	Cu-YW-18-Me	H_3nota^{29}
6.6	9.20	10.04	9.92	12.15	9.53	
7.4	9.18	9.80	9.68	12.14	9.17	17.6

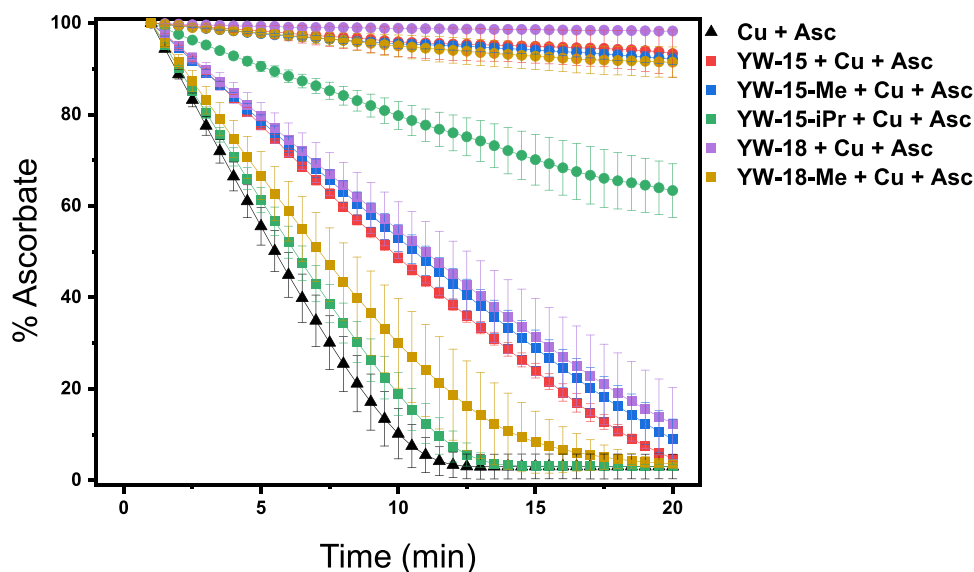


Figure 6. Capacity of ligands to prevent Cu^{2+} -induced radical formation as determined by the CIAC (Cu^{2+} -induced antioxidant capacity) assay over 20 min ($[\text{Cu}^{2+}] = 10 \mu\text{M}$, $[\text{ascorbate}] = 100 \mu\text{M}$, for square points, $[\text{antioxidant}] = 10 \mu\text{M}$; for round points, $[\text{antioxidant}] = 25 \mu\text{M}$).

formation by monitoring the presence of ascorbate in solution following addition of an oxidizing agent. Utilization of this assay with Cu^{2+} as an oxidizing agent gives insight into stability and redox potential of the complexes by measuring the consumption by oxidation of ascorbate. Smaller amounts of ascorbate consumption indicate that complexation has shifted the redox potential of the Cu^{2+} , preventing the metal from oxidizing ascorbate. Ascorbate remaining in solution also indicates the stability of the complex, preventing the Cu^{2+} from returning to solution and oxidizing ascorbate. Each ligand studied indicated some ability to prevent radical formation, with ligands YW-15, YW-15-Me, YW-18, and YW-18-Me showing greater than 90% ascorbate remaining in solution after 20 min (Figure 6). By comparison, YW-15-iPr showed a lesser ability to prevent radical formation at higher concentrations, with approximately 60% of ascorbate remaining in solution after 20 min. At lower concentrations, the antioxidant capacity of the ligands is significantly reduced, with less than 20% of ascorbate remaining in solution after 20 min for all ligands. These results indicate that ligand YW-15-iPr has the lowest ability to prevent Cu^{2+} -induced oxidative stress when complexed with $\text{Cu}(\text{II})$, suggesting poor potential for use as a PET tracer. However, the ability of other ligands tested to prevent the inducement of such oxidative stress indicates that they should not be eliminated from consideration as ^{64}Cu -based PET tracers.

EPR Spectra of Copper Complexes. To further characterize the Cu-BFC complexes, their X-band EPR spectra were recorded in frozen glasses at 77 K. The Cu^{2+} complexes were prepared immediately before the EPR experiment by reacting ligand with 0.8 equiv CuCl_2 . The EPR spectrum of Cu-YW-15-Me in a 1:3 (v:v) MeCN:PrCN glass reveals a pseudoaxial pattern with three different g values: $g_z = 2.240$, $A_z(\text{Cu}) = 162 \text{ G}$, $g_y = 2.057$, and $g_x = 2.032$ (Figure 7). The EPR spectra of Cu-YW-15, Cu-YW-15-iPr, Cu-YW-18, Cu-YW-18-Me, and Cu-YW-18-tBu were obtained the same way and exhibit similar EPR patterns as Cu-YW-15-Me (Table 6, Figure S11).⁴³ Each complex exhibits an EPR pattern characteristic of a mononuclear Cu^{2+} complex, indicating the

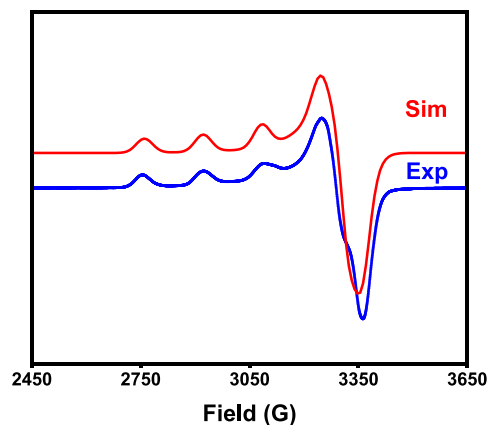


Figure 7. Experimental and simulated EPR spectra of the Cu-YW-15-Me complex in 1:3 MeCN:PrCN glass at 77 K. The following parameters were used for the simulation: $g_z = 2.240$, $A_z(\text{Cu}) = 162 \text{ G}$, $g_y = 2.032$, and $g_x = 2.057$.

Table 6. EPR Parameter of Cu(II)-BFC Complexes of Spectra in Figure 7 and Figure S12

ligand	g_z	A_z	g_y	g_x
YW-15	2.233	155 G	2.100	2.015
YW-15-Me	2.240	162 G	2.057	2.032
YW-15-iPr	2.238	162 G	2.090	2.005
YW-18	2.232	165 G	2.078	2.022
YW-18-Me	2.245	163 G	2.100	2.010
YW-18-tBu	2.248	162 G	2.072	2.024

stability and inaptitude toward dimerization of these Cu complexes in solution.

Radiolabeling of BFCs. The radiolabeling of compounds YW-15, YW-15-Me, YW-18, and YW-18-tBu was performed using $^{64}\text{CuCl}_2$ and employing conditions described in the Supporting Information. The BFCs were readily labeled with ^{64}Cu under mild conditions. Quality control assays were conducted using HPLC and/or TLC; HPLC retention times were observed in the range of 10.5–11.2 min for the ^{64}Cu -

radiolabeled complexes (Figure S13). All radiochemical purities were >95% within minutes at 95 °C, with specific activities of 100 Ci/mmol or greater. Therefore, all radiolabeled complexes were used directly without further purification.

One important factor of diagnostic agents for AD is the ability to penetrate the BBB. The octanol/PBS partition coefficient values $\log D$ were determined for ^{64}Cu -radiolabeled BFCs (Table 7). A decreasing trend of $\log D$ values with less

Table 7. Molecular Weights (MWs) of Ligands and Measured $\log D$ Values for the Corresponding ^{64}Cu -Radiolabeled Complexes

ligand	MW (g·mol ⁻¹)	$\log D$
YW-15	667.2	1.43 ± 0.09
YW-15-Me	681.2	1.29 ± 0.04
YW-15-iPr	709.9	1.05 ± 0.02
YW-18	725.3	1.34 ± 0.03
YW-18-Me	739.3	1.70 ± 0.08
YW-18-tBu	782.3	1.85 ± 0.07

bulky alkyl groups was observed. Gratifyingly, the obtained $\log D$ values for ^{64}Cu -radiolabeled complexes, with the exception of YW-15-iPr, are promising, in the range of 1.29–1.85, which suggests their potential ability to cross the BBB via passive diffusion.⁴¹ Interestingly, the ^{64}Cu complex of YW-18, which contains two phenol groups and one carboxylic acid group, has a positive $\log D$ value of 1.34 ± 0.03 and thus is likely to cross the BBB. The hydrophilicity of the carboxylic acid group is normally not favorable for BBB permeability, yet in this case, we propose that solution one of the two phenol groups is deprotonated to become a phenolate, forming a neutral Cu(II) complex along with the carboxylic acid group in YW-18 and therefore is beneficial for BBB penetration. Interestingly, this correlates well with the $\log D$ values of 1.24 and 1.66 obtained for the ^{68}Ga (III) complexes of YW-15 and YW-18, respectively,²⁸ vs the values of 1.43 and 1.34 for the corresponding ^{64}Cu (II) complexes reported herein (Table 7), further supporting that the phenol groups could become deprotonated to accommodate that charge of the chelated metal ion and thus lead to lipophilic metal complexes that have the potential to cross the BBB, especially for the dicationic ^{64}Cu (II) ion.

For all BFCs other than YW-15-iPr, the $\log D$ values of the complexes were observed to be greater than the $\log D$ of the BFC itself. While the molecular weights of the ligands are greater than those of the BFCs and higher than optimal molecular weight ranges for BBB permeability, previously reported ligands with similar molecular weights have exhibited good BBB permeability.^{22,23} We propose that the $\log D$ of the Cu-YW-15-iPr complex is lower than the $\log D$ of the ligand due to a more complex species distribution, as shown above for the species distribution titrations. Additionally, the $\log D$ of the Cu-YW-18-tBu complex was observed to be only marginally higher than that of the Cu-YW-18-Me complex, and thus it was not employed in subsequent biodistribution studies.

Overall, all the tested BFCs have desirable $\log D$ values (ideally larger than 1), and thus we proceeded with their further characterization, including autoradiography and biodistribution studies.

autoradiography Studies. *Ex vivo* autoradiography studies using brain sections from 11 month old 5xFAD and aged-matched WT mice were conducted to determine the specific binding of the ^{64}Cu -labeled BFCs to the amyloid plaques. The brain sections were stained, washed, and imaged as described in the Supporting Information. Unfortunately, YW-15-Me and YW-18-tBu exhibit appreciable background intensity (Figure 8A, first row and Figure 8B, red), indicating nonspecific binding. In the case of 5xFAD mouse brain sections, we observed an increased autoradiography intensity for all complexes (Figure 8A, second row and Figure 8B, blue), with YW-18-tBu exhibiting the highest overall intensity, while YW-15, YW-18, and YW-18-Me exhibit the largest fold increase (~4) for 5xFAD vs WT brain sections (Figure 8B).

The specific binding to amyloid plaques of the radiolabeled BFCs was further confirmed by blocking the brain sections with a nonradioactive blocking agent B₁ (Figure S14), and a remarkable decrease in autoradiography intensity was observed (Figure 8A, third row and Figure 8B, green).

Biodistribution Studies. Encouraged by the promising *in vitro* studies, *in vivo* biodistribution experiments were performed to investigate the pharmacokinetics of ^{64}Cu -radiolabeled BFCs, using normal CD-1 and Tg2576 mice as described in the Supporting Information. The retention and accumulation of the ^{64}Cu -radiolabeled YW-15, YW-15-Me, and YW-18 complexes in selected organs of CD-1 mice were evaluated at 2, 60, and 240 min after tracer administration (Figure 9, Table 8). Ligands YW-15, YW-15-Me, and YW-18

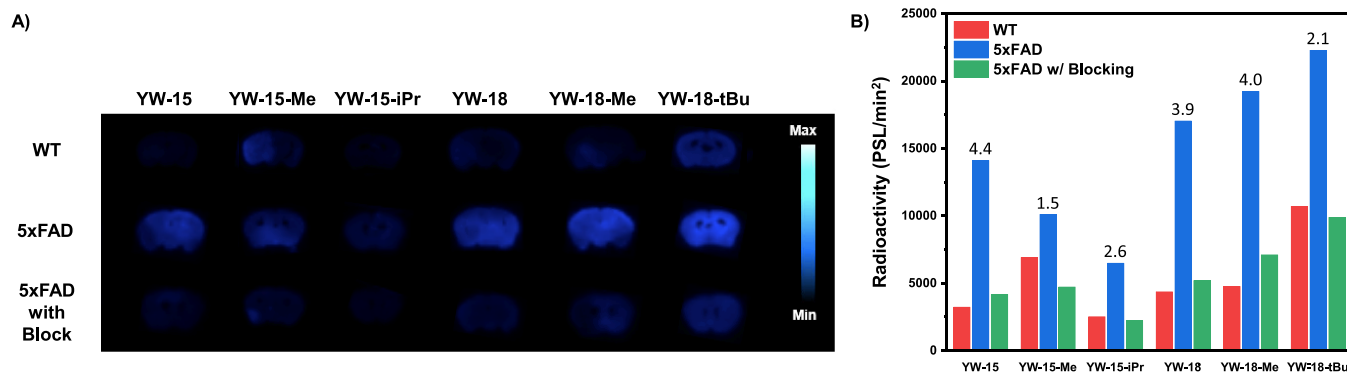


Figure 8. Autoradiography of brain sections of WT and 5xFAD transgenic mice stained with ^{64}Cu -radiolabeled complexes, in the absence and presence with $A\beta$ specific blocking agent B₁.⁴³ (A) Images of brain sections and (B) average radioactivity of brain sections in the autoradiography images (where numbers indicate intensity ratio of 5xFAD to WT for each complex, $n = 1$).

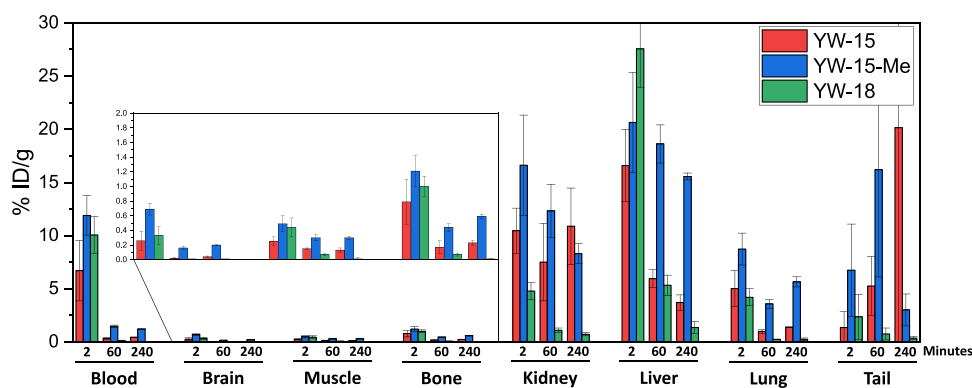


Figure 9. Uptake (%ID/g) of ^{64}Cu radiolabeled complexes from *in vivo* biodistribution studies in mouse organs. Studies were conducted in CD-1 normal female mice aged 5–7 weeks, $n = 3$.

Table 8. Overall Biodistribution Results of ^{64}Cu -Labeled YW-15, YW-15-Me, and YW-18 for the Three Time Points Evaluated (2, 60, and 240 min; % Injected Dose per Gram, Mean \pm SEM for Duplicate)^a

	YW-15 2 min	YW-15 1 h	YW-15 4 h	YW-15-Me 2 min	YW-15-Me 1 h	YW-15-Me 4 h	YW-18 2 min	YW-18 1 h	YW-18 4 h
blood	6.71 ± 2.84	0.33 ± 0.09	0.43 ± 0.03	11.90 ± 1.85	1.47 ± 0.12	1.21 ± 0.06	10.06 ± 1.72	0.11 ± 0.01	0.05 ± 0.01
brain	0.26 ± 0.13	0.02 ± 0.01	0.04 ± 0.01	0.69 ± 0.08	0.16 ± 0.02	0.20 ± 0.01	0.33 ± 0.12	0.01 ± 0.00	0.01 ± 0.00
muscle	0.25 ± 0.06	0.15 ± 0.01	0.13 ± 0.03	0.49 ± 0.11	0.30 ± 0.04	0.30 ± 0.02	0.44 ± 0.13	0.07 ± 0.01	0.01 ± 0.02
bone	0.79 ± 0.31	0.17 ± 0.09	0.23 ± 0.03	1.21 ± 0.21	0.44 ± 0.05	0.59 ± 0.03	1.00 ± 0.14	0.07 ± 0.02	0.01 ± 0.01
kidney	10.46 ± 2.13	7.51 ± 3.64	10.89 ± 3.58	16.62 ± 4.72	12.33 ± 2.51	8.31 ± 0.93	4.79 ± 0.79	1.09 ± 0.22	0.72 ± 0.14
liver	16.59 ± 3.40	5.96 ± 0.84	3.71 ± 0.72	20.64 ± 4.72	18.62 ± 1.80	15.56 ± 0.32	27.56 ± 3.60	5.33 ± 0.95	1.36 ± 0.58
lung	5.02 ± 1.70	0.99 ± 0.17	1.38 ± 0.31	8.74 ± 1.50	3.57 ± 0.43	5.65 ± 0.47	4.20 ± 0.80	0.25 ± 0.01	0.24 ± 0.13
tail	1.36 ± 1.50	5.26 ± 2.78	20.16 ± 23.41	6.75 ± 4.34	16.21 ± 10.1	3.01 ± 1.50	2.36 ± 2.12	0.75 ± 0.56	0.36 ± 0.15

^aStudies conducted in normal CD-1 female mice aged 5–7 weeks, $n = 3$

were chosen for biodistribution studies to assess how changes to the ligand N-substituent impact the *in vivo* properties of the corresponding complexes. In WT mice, YW-15, YW-15-Me, and YW-18 showed moderate brain uptake at 2 min post-injection, followed by rapid washout (Figure 9, Table 8). ^{64}Cu -YW-15 showed a brain uptake of $0.26 \pm 0.13\%$ ID/g at 2 min post-injection, which dropped to $\sim 0.04 \pm 0.01\%$ ID/g at 60 and 240 min post-injection, ^{64}Cu -YW-15-Me showed the brain uptake of $0.47 \pm 0.12\%$ ID/g at 2 min post-injection which dropped to $\sim 0.15\%$ ID/g 60 and 240 min post-injection, and ^{64}Cu -YW-18 showed brain uptake of $0.33 \pm 0.12\%$ ID/g at 2 min post-injection, which then dropped to $\sim 0.01\%$ ID/g at 60 and 240 min post-injection (Figure 9, Table 8). Interestingly, ^{64}Cu -YW-15-Me has the highest %ID/g in the brain at each time point, although it has neither the lowest nor the highest molecular weight of the three similarly lipophilic complexes studied. This indicates factors outside lipophilicity and molecular weight impact the biodistribution profile of these complexes. The brain to blood ratio results (Figure 10) suggest that the retention of ^{64}Cu complexes in the brain slightly increases with time, possibly due to their favorable lipophilicity.

Overall, these biodistribution studies suggest that the ^{64}Cu -radiolabeled TACN-based complexes can cross the BBB and

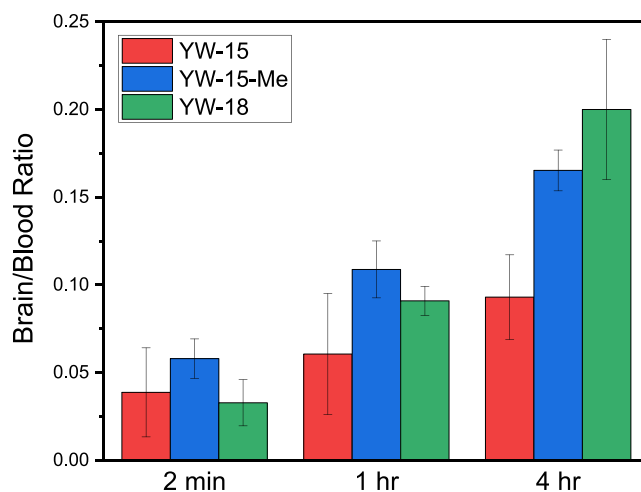


Figure 10. Brain-to-blood ratio results from the *in vivo* biodistribution study at 2 min, 1 h, and 4 h post-injection in CD-1 normal female mice aged 5–7 weeks, $n = 3$.

thus could serve as a PET imaging agents for detecting A β plaque burden *in vivo* following further optimization of blood–brain-barrier permeability. Importantly, the rapid clearance from the brain of WT mice indicate that this radiolabeled BFC

does not release ^{64}Cu ions in the brain to an appreciable extent and thus should not lead to a significant background PET signal in healthy controls.

CONCLUSIONS

Reported herein is a series of bifunctional chelators (BFCs) consisting of two $A\beta$ -binding fragments and a TACN metal-chelating fragment. These BFCs exhibit remarkable labeling of $A\beta$ species in *ex vivo* 5xFAD mouse brain section staining. Interestingly, in comparison with the previously published BFCs, the inclusion of an additional $A\beta$ -binding fragment has minimal impact on the binding affinity toward $A\beta$ plaques, which remained in the 100 nM range.²⁶ For comparison, the K_i of ^{18}F -Florbetaben, an FDA-approved PET imaging agent used in AD diagnosis, is 6.7 nM,¹⁴ indicating that further optimization of the amyloid-targeting fragment of these complexes would be beneficial. While the inclusion of additional $A\beta$ -binding fragments did not increase the affinity for $A\beta$ plaques as anticipated, a desirable impact of increased BFC lipophilicity was observed, making them more favorable for BBB penetration. The increased lipophilicity is maintained for the corresponding ^{64}Cu complexes, which have slightly higher $\log D$ values than previously published complexes with one $A\beta$ -binding fragment and one carboxylate ester arm²⁶ and significantly higher $\log D$ values than previously published complexes with one $A\beta$ -binding fragment and two carboxylate ester arms.²⁷

The BFCs were additionally modified by incorporation of *N*-alkyl or *N*-carboxylate methyl ester arms on the TACN backbone. Changes of the *N*-alkyl substituent from hydrogen to methyl to isopropyl decreased the $\log D$ of the overall complexes, likely due to the bulky alkyl substituents interfering with ability of the phenols to be involved in coordination to the Cu center. This indicates that inclusion of larger alkyl groups has little to no benefit on the lipophilicity of these complexes, while alkyl groups larger than methyl may not be beneficial due to the detrimental effect on Cu^{2+} binding affinity. In addition, a minimal benefit to the lipophilicity of the complexes was observed upon changes to the *N*-methyl ester substituents, while negative impacts on the Cu^{2+} complex stability of the BFCs were observed upon alkylation of the carboxylic acid with a methyl or *tert*-butyl ester group. Interestingly, the $p\text{Cu}$ values of the alkyl esters were similar to values for the BFCs containing *N*-alkyl arms. **Cu-YW-18** has the highest $p\text{Cu}$ value of all BFCs described herein, similar $p\text{Cu}$ values for the previously reported ligand with two carboxylic acids, and closer to the $p\text{Cu}$ value reported for **H₃nota**, a strong chelator of Cu^{2+} .^{27,29} Taken together these results indicate that carboxylate ester arms had minimal impact on Cu^{2+} complex stability, but carboxylic acid substituents increase Cu^{2+} complex stability. However, the inclusion of more than one carboxylic acid substituent did not further increase the stability of the Cu^{2+} complex stability. Encouragingly, the Cu^{2+} complexes of BFCs with carboxylic acid substituents did not show significantly decreased lipophilicity, as assessed by $\log D$ or brain uptake in biodistribution studies,²⁷ indicating that their presence does not negatively impact BBB penetrability.

Of the complexes investigated herein, ^{64}Cu -YW-15-Me showed the most promising brain uptake in CD-1 mice, with a maximum %ID/g of 0.47 ± 0.12 at 2 min post-injection and with minor increases in brain/blood ratios from 2 min to 4 h, indicating minimal complex retention in the brain. ^{64}Cu -based

imaging agents reported in the literature vary in brain uptake values from approximately 0.3 %ID/g in some cyclen systems to approximately 0.75–2.5 %ID/g in some ATSM systems, with the BFCs described herein more closely resemble the moderate brain uptake of the cyclen systems.²⁰ The BFCs described herein and their ^{64}Cu complexes, when compared to previously published compounds,^{26,27} point toward the need of further development of TACN-based ligands, with one amyloid-targeting fragment to limit the overall molecular weight, a small *N*-substituent such as hydrogen or methyl, and a carboxylic acid arm to increase the ^{64}Cu complex stability. This indicates a direction for the optimization of ^{64}Cu -TACN-based ligand to optimize BBB penetrability and increase the affinity for amyloid plaques, prior to use for *in vivo* PET imaging applications.

ASSOCIATED CONTENT

Supporting Information

The Supporting Information is available free of charge at <https://pubs.acs.org/doi/10.1021/acs.inorgchem.2c02740>.

Additional experimental details materials, methods, characterization, and data including spectrophotometric titrations, Job's plots, UV–vis and fluorescence spectra, and HPLC chromatograms of radiolabeling assays (PDF)

AUTHOR INFORMATION

Corresponding Authors

Buck E. Rogers – Department of Radiation Oncology, Washington University School of Medicine, St. Louis, Missouri 63108, United States; orcid.org/0000-0001-8189-1797; Email: b.rogers@wustl.edu

Liviu M. Mirica – Department of Chemistry, University of Illinois at Urbana-Champaign, Urbana, Illinois 61801, United States; Hope Center for Neurological Disorders, Washington University School of Medicine, St. Louis, Missouri 63110, United States; orcid.org/0000-0003-0584-9508; Email: mirica@illinois.edu

Authors

Karna Terpstra – Department of Chemistry, University of Illinois at Urbana-Champaign, Urbana, Illinois 61801, United States

Yujue Wang – Department of Chemistry, University of Illinois at Urbana-Champaign, Urbana, Illinois 61801, United States

Truc T. Huynh – Department of Radiation Oncology, Washington University School of Medicine, St. Louis, Missouri 63108, United States; Department of Chemistry, Washington University, St. Louis, Missouri 63130, United States

Nilantha Bandara – Department of Radiation Oncology, Washington University School of Medicine, St. Louis, Missouri 63108, United States

Hong-Jun Cho – Department of Chemistry, University of Illinois at Urbana-Champaign, Urbana, Illinois 61801, United States

Complete contact information is available at:

<https://pubs.acs.org/doi/10.1021/acs.inorgchem.2c02740>

Author Contributions

[○]K.T. and Y.W. contributed equally.

Notes

The authors declare no competing financial interest.

ACKNOWLEDGMENTS

This work was supported by research funding from the NIH (R01GM114588 to L.M.M.). We thank the small animal imaging facilities at Washington University School of Medicine for excellent technical assistance and the Isotope Production Group at Washington University for the production of ^{64}Cu .

REFERENCES

- (1) Jakob-Roetne, R.; Jacobsen, H. Alzheimer's Disease: From Pathology to Therapeutic Approaches. *Angew. Chem., Int. Ed.* **2009**, *48*, 3030–3059.
- (2) Savelieff, M. G.; Nam, G.; Kang, J.; Lee, H. J.; Lee, M.; Lim, M. H. Development of Multifunctional Molecules as Potential Therapeutic Candidates for Alzheimer's Disease, Parkinson's Disease, and Amyotrophic Lateral Sclerosis in the Last Decade. *Chem. Rev.* **2019**, *119*, 1221–1322.
- (3) Tiwari, S.; Atluri, V.; Kaushik, A.; Yndart, A.; Nair, M. Alzheimer's disease: pathogenesis, diagnostics, and therapeutics. *Int. J. Nanomed.* **2019**, *Volume 14*, 5541–5554.
- (4) De Strooper, B.; Karran, E. The Cellular Phase of Alzheimer's Disease. *Cell* **2016**, *164*, 603–615.
- (5) DeTure, M. A.; Dickson, D. W. The neuropathological diagnosis of Alzheimer's disease. *Mol. Neurodegener.* **2019**, *14*, 32.
- (6) Hickey, J. L.; Lim, S.; Hayne, D. J.; Paterson, B. M.; White, J. M.; Villemagne, V. L.; Roselt, P.; Binns, D.; Cullinane, C.; Jeffery, C. M.; Price, R. I.; Barnham, K. J.; Donnelly, P. S. Diagnostic Imaging Agents for Alzheimer's Disease: Copper Radiopharmaceuticals that Target A β Plaques. *J. Am. Chem. Soc.* **2013**, *135*, 16120–16132.
- (7) Pietrzak, K.; Czarnecka, K.; Mikiciuk-Olasik, E.; Szymanski, P. New Perspectives of Alzheimer Disease Diagnosis - the Most Popular and Future Methods. *Med. Chem.* **2018**, *14*, 34–43.
- (8) Nasrallah, I.; Dubroff, J. An Overview of PET Neuroimaging. *Semin. Nucl. Med.* **2013**, *43*, 449–461.
- (9) Mathis, C.; Wang, Y.; Klunk, W. Imaging β -amyloid plaques and neurofibrillary tangles in the aging human brain. *Curr. Pharm. Des.* **2004**, *10*, 1469–1492.
- (10) Serdons, K.; Verduyck, T.; Vanderghinste, D.; Borghgraef, P.; Cleynhens, J.; Van Leuven, F.; Kung, H.; Bormans, G.; Verbruggen, A. 11C-labelled PIB analogues as potential tracer agents for in vivo imaging of amyloid beta in Alzheimer's disease. *Eur. J. Med. Chem.* **2009**, *44*, 1415–1426.
- (11) Serdons, K.; Terwinghe, C.; Vermaelen, P.; Van Laere, K.; Kung, H.; Mortelmans, L.; Bormans, G.; Verbruggen, A. Synthesis and evaluation of ^{18}F -labeled 2-phenylbenzothiazoles as positron emission tomography imaging agents for amyloid plaques in Alzheimer's disease. *J. Med. Chem.* **2009**, *52*, 1428–1437.
- (12) Choi, S. R.; Golding, G.; Zhuang, Z.; Zhang, W.; Lim, N.; Hefti, F.; Benedum, T. E.; Kilbourn, M. R.; Skovronsky, D.; Kung, H. F. Preclinical Properties of 18F-AV-45: A PET Agent for A β Plaques in the Brain. *J. Nucl. Med.* **2009**, *50*, 1887–1894.
- (13) Uzegbunam, B. C.; Librizzi, D.; Hooshyar Yousefi, B. PET Radiopharmaceuticals for Alzheimer's Disease and Parkinson's Disease Diagnosis, the Current and Future Landscape. *Molecules* **2020**, *25*, 977.
- (14) Richards, D.; Sabbagh, M. N. Florbetaben for PET Imaging of Beta-Amyloid Plaques in the Brain. *Neurol. Ther.* **2014**, *3*, 79–88.
- (15) Conti, M.; Eriksson, L. Physics of pure and non-pure positron emitters for PET: a review and a discussion. *EJNMMI Phys* **2016**, *3*, 8.
- (16) Wadas, T. J.; Wong, E. H.; Weisman, G. R.; Anderson, C. J. Coordinating Radiometals of Copper, Gallium, Indium, Yttrium, and Zirconium for PET and SPECT Imaging of Disease. *Chem. Rev.* **2010**, *110*, 2858–2902.
- (17) Máté, G.; Šimeček, J.; Pniok, M.; Kertész, I.; Notni, J.; Wester, H. J.; Galuska, L.; Hermann, P. The influence of the combination of carboxylate and phosphinate pendant arms in 1,4,7-triazacyclononane-based chelators on their ^{68}Ga labelling properties. *Molecules* **2015**, *20*, 13112–13126.
- (18) Joshi, T.; Kubeil, M.; Nsubuga, A.; Singh, G.; Gasser, G.; Stephan, H. Harnessing the Coordination Chemistry of 1,4,7-Triazacyclononane for Biomimicry and Radiopharmaceutical Applications. *Chempluschem* **2018**, *83*, 554–564.
- (19) Blake, A. J.; Danks, J. P.; Li, W. S.; Lippolis, V.; Schroder, M. Synthesis and characterisation of pendant-arm amino derivatives of 1,4,7-triazacyclononane and alkyl-bridged bis(1,4,7-triazacyclononane) macrocycles and complexation to Cu(II). *J. Chem. Soc. Dalton Trans.* **2000**, *17*, 3034–3040.
- (20) Krasnovskaya, O.; Spector, D.; Zlobin, A.; Pavlov, K.; Gorelkin, P.; Erofeev, A.; Beloglazkina, E.; Majouga, A. Metals in Imaging of Alzheimer's Disease. *Int. J. Mol. Sci.* **2020**, *21*, 9190.
- (21) Sharma, A. K.; Schultz, J. W.; Prior, J. T.; Rath, N. P.; Mirica, L. M. Coordination Chemistry of Bifunctional Chemical Agents Designed for Applications in (^{64}Cu) PET Imaging for Alzheimer's Disease. *Inorg. Chem.* **2017**, *56*, 13801–13814.
- (22) Bandara, N.; Sharma, A. K.; Krieger, S.; Schultz, J. W.; Han, B. H.; Rogers, B. E.; Mirica, L. M. Evaluation of ^{64}Cu -based Radiopharmaceuticals That Target A β Peptide Aggregates as Diagnostic Tools for Alzheimer's Disease. *J. Am. Chem. Soc.* **2017**, *139*, 12550–12558.
- (23) Cho, H. J.; Huynh, T. T.; Rogers, B. E.; Mirica, L. M. Design of a multivalent bifunctional chelator for diagnostic (^{64}Cu) PET imaging in Alzheimer's disease. *Prod. Natl. Acad. Sci. U. S. A.* **2020**, *117*, 30928–30933.
- (24) Huang, Y.; Cho, H.-J.; Bandara, N.; Sun, L.; Tran, D.; Rogers, B. E.; Mirica, L. M. Metal-chelating benzothiazole multifunctional compounds for the modulation and ^{64}Cu PET imaging of A β aggregation. *Chem. Sci.* **2020**, *11*, 7789–7799.
- (25) Sun, L.; Chi, H.-J.; Sen, S.; Arango, A. S.; Huynh, T. T.; Huang, Y.; Bandara, N.; Rogers, B. E.; Tajkhorshid, E.; Mirica, L. M. Amphiphilic Distyrylbenzene Derivatives as Potential Therapeutic and Imaging Agents for the Soluble Amyloid- β Oligomers in Alzheimer's Disease. *J. Am. Chem. Soc.* **2021**, *143*, 10462–10476.
- (26) Wang, Y.; Huynh, T. T.; Cho, H.-J.; Wang, Y.-C.; Rogers, B. E.; Mirica, L. M. Amyloid β -Binding Bifunctional Chelators with Favorable Lipophilicity for ^{64}Cu Positron Emission Tomography Imaging in Alzheimer's Disease. *Inorg. Chem.* **2021**, *60*, 12610–12620.
- (27) Wang, Y.; Huynh, T. T.; Bandara, N.; Cho, H.-J.; Rogers, B. E.; Mirica, L. M. 2-(4-Hydroxyphenyl)benzothiazole Dicarboxylate Ester TACN Chelators for ^{64}Cu PET imaging in Alzheimer's Disease. *Dalton Trans.* **2022**, *51*, 1216–1224.
- (28) Huynh, T. T.; Wang, Y.; Terpstra, K.; Cho, H.-J.; Mirica, L. M.; Rogers, B. E. ^{68}Ga -Labeled Benzothiazole Derivatives for Imaging A β Plaques in Cerebral Amyloid Angiopathy. *ACS Omega* **2022**, *7*, 20339–20346.
- (29) Guillou, A.; Lima, L. M. P.; Roger, M.; Esteban-Gómez, D.; Delgado, R.; Platas-Iglesias, C.; Patinec, V.; Tripier, R. 1,4,7-Triazacyclononane-Based Bifunctional Picolinate Ligands for Efficient Copper Complexation. *Eur. J. Inorg. Chem.* **2017**, *2017*, 2435–2443.
- (30) Terpstra, K.; Wang, Y.; Huynh, T. T.; Bandara, N.; Cho, H.-J.; Rogers, B. E.; Mirica, L. M., Divalent 2-(4-Hydroxyphenyl)-benzothiazole Bifunctional Chelators for ^{64}Cu PET Imaging in Alzheimer's Disease. *ChemRxiv preprint*, **2022**, DOI: 10.26434/chemrxiv-2022-06vz9, (accessed November 17, 2022).
- (31) Oakley, H.; Cole, S. L.; Logan, S.; Maus, E.; Shao, P.; Craft, J.; Guillozet-Bongaarts, A.; Ohno, M.; Disterhoft, J.; Van Eldik, L.; Berry, R.; Vassar, R. Intra-neuronal β -amyloid aggregates, neurodegeneration, and neuron loss in transgenic mice with five familial Alzheimer's disease mutations: potential factors in amyloid plaque formation. *J. Neurosci.* **2006**, *26*, 10129–10140.
- (32) Drummond, E.; Wisniewski, T. Alzheimer's disease: experimental models and reality. *Acta Neuropathol.* **2017**, *133*, 155–175.
- (33) Klunk, W. E.; Pettegrew, J. W.; Abraham, D. J. Quantitative evaluation of congo red binding to amyloid-like proteins with a beta-

pleated sheet conformation. *J. Histochem. Cytochem.* **1989**, *37*, 1273–1281.

(34) Yakupova, E. I.; Bobyleva, L. G.; Vikhlyantsev, I. M.; Bobylev, A. G. Congo Red and amyloids: history and relationship. *Biosci. Rep.* **2019**, *39*, 1.

(35) Schwetye, K. E.; Cirrito, J. R.; Esparza, T. J.; Mac Donald, C. L.; Holtzman, D. M.; Brody, D. L. Traumatic Brain Injury Reduces Soluble Extracellular Amyloid- β in Mice: A Methodologically Novel Combined Microdialysis-Controlled Cortical Impact Study. *Neurobiol. Dis.* **2010**, *40*, 555–564.

(36) Esparza, T. J.; Wildburger, N. C.; Jiang, H.; Gangolli, M.; Cairns, N. J.; Bateman, R. J.; Brody, D. L. Soluble Amyloid-beta Aggregates from Human Alzheimer's Disease Brains. *Sci. Rep.* **2016**, *6*, 38187.

(37) Sun, L.; Sharma, A. K.; Han, B.-H.; Mirica, L. M. Amentoflavone: A Bifunctional Metal Chelator that Controls the Formation of Neurotoxic Soluble A β 42 Oligomers. *ACS Chem. Neurosci.* **2020**, *11*, 2741–2752.

(38) Perrin, R. J.; Fagan, A. M.; Holtzman, D. M. Multimodal Techniques for Diagnosis and Prognosis of Alzheimer's Disease. *Nature* **2009**, *461*, 916–922.

(39) Fagan, A. M.; Holtzman, D. M. Cerebrospinal fluid biomarkers of Alzheimer's disease. *Biomark. Med.* **2010**, *4*, 51–63.

(40) Dischino, D. D.; Welch, M. J.; Kilbourn, M. R.; Raichle, M. E. Relationship between Lipophilicity and Brain Extraction of C-11-Labeled Radiopharmaceuticals. *J. Nucl. Med.* **1983**, *24*, 1030–1038.

(41) Mikitsh, J. L.; Chacko, A. M. Pathways for small molecule delivery to the central nervous system across the blood-brain barrier. *Pers. Med. Chem.* **2014**, *6*, 11–24.

(42) McInnes, L. E.; Noor, A.; Roselt, P. D.; McLean, C. A.; White, J. M.; Donnelly, P. S. A Copper Complex of a Thiosemicarbazone-Pyridylhadazone Ligand Containing a Vinylpyridine Functional Group as a Potential Imaging Agent for Amyloid- β Plaques. *Austr. J. Chem.* **2019**, *72*, 827–834.

(43) See [Supporting Information](#).

Recommended by ACS

Probing Unexpected Reactivity in Radiometal Chemistry: Indium-111-Mediated Hydrolysis of Hybrid Cyclen-Hydroxypyridinone Ligands

Charlotte Rivas, Michelle T. Ma, *et al.*

MARCH 17, 2023

INORGANIC CHEMISTRY

[READ](#)

Characteristic Evaluation of a ^{14}C -Labeled Leucine Analog, $1-\alpha$ -[$5-^{14}\text{C}$]methylleucine, as a Tracer for Brain Tumor Imaging by Positron Emission Tomography

Tsuyoshi Tahara, Hirotaka Onoe, *et al.*

FEBRUARY 20, 2023

MOLECULAR PHARMACEUTICS

[READ](#)

$\text{H}_3\text{TPAN-Triazole-Bn-NH}_2$: Tripicolinate Clicked-Bifunctional Chelate for [^{225}Ac]/[^{111}In] Theranostics

Luke Wharton, Chris Orvig, *et al.*

NOVEMBER 15, 2022

BIOCONJUGATE CHEMISTRY

[READ](#)

Replenishment in the Family of Rhenium Chalcobromides; Synthesis and Structure of Molecular $\{\text{Re}_4\text{S}_4\}\text{Br}_8(\text{TeBr}_2)_4$, Dimeric $[\{\text{Re}_4\text{S}_4\}\text{Br}_8(\text{TeBr}_2)_2]$, and Polymeric $\{\text{Re}_4\text{S}_4\}\text{B}...$

Spartak S. Yarovoy, Nikolay G. Naumov, *et al.*

DECEMBER 05, 2022

INORGANIC CHEMISTRY

[READ](#)

[Get More Suggestions >](#)